Electromagnetic radiation in hot QCD matter: Rates, electric conductivity, flavor susceptibility, and diffusion

Chang-Hwan Lee[1,2] and Ismail Zahed[2]

[1]*Department of Physics, Pusan National University, Busan 609-735, South Korea*
[2]*Department of Physics and Astronomy, Stony Brook University, New York 11794, USA*

We discuss the general features of the electromagnetic radiation from a thermal hadronic gas as constrained by chiral symmetry. The medium effects on the electromagnetic spectral functions and the partial restoration of chiral symmetry are quantified in terms of the pion densities. The results are compared with the electromagnetic radiation from a strongly interacting quark-gluon plasma in terms of the leading gluon condensate operators. We use the spectral functions as constrained by the emission rates to estimate the electric conductivity, the light flavor susceptibility and diffusion constant across the transition from the correlated hadronic gas to a strongly interacting quark-gluon plasma.

I. INTRODUCTION

One of the chief objectives of the ultrarelativistic heavy ion program at BNL Relativistic Heavy Ion Collider (RHIC) and CERN Large Hadron Collider (LHC) is to excite enough of the QCD vacuum in the form of a quark-gluon plasma. The plasma expands and hadronize relatively quickly making its identification only implicit through the high hadronic multiplicities or electromagnetic emissivities [1–10].

Electromagnetic emissions in the form of dileptons or photons occur throughout the life-time of the expanding fireball. The early stages are dominated by the emission from the partonic constituents, while the late stages of the emission are dominated by the hadronic constituents. Both the early and late stages are well described by a hydrodynamical fireball. In this paper, instead of integrating over the space-time of the evolving fireball, we discuss the basics of the electromagnetic emissivities from a hadronic gas [11–16] and a strongly coupled plasma (sQGP) which is described in terms of Born diagrams [17] corrected by leading order gluon condensates [18–20]. The comparison with the newly reported lattice simulations of the electromagnetic spectral functions at zero momentum puts some constraints on the importance on the gluon condensates [21–23].

Dilepton and photon emissions are the results of many reaction processes involving the quark-gluon plasma in the early stage and hadrons and the strong character of their interactions in the later stage. For the emissions from the hadronic gas, the only organizational principles are broken chiral symmetry and gauge invariance, both of which are difficult to assert in individual reaction processes. In the spectral analysis [24,25], if hadrons thermalize with the pions and nucleons as the only strongly stable constituents, there is a way to systematically organize the electromagnetic emissivities by expanding them not in terms of processes but rather in terms of final hadronic states. Then the emissivities from the hadronic gas can be represented by spectral functions by chiral reduction [11,12]. These spectral functions are either tractable from other experiments or amenable to resonance saturation [26]. The spectral analysis allows us to represent the partial chiral symmetry restoration in terms of the mixing between vector and axial correlators.

In Sec. II, we review the spectral function approach to the photon and dilepton rates emphasizing the nature of the dynamical restoration of the partially broken chiral symmetry in the hadronic fireball through the mixing of vector and axial correlators. We also discuss the electric conductivity and the quark number susceptibilities in the correlated hadronic gas near the chiral transition. In Sec. III we review the sQGP corrected by the soft electric and magnetic condensates and show that they may enhance the soft photon and dilepton emissions. The electric conductivity and the flavor diffusion constant in the sQGP are derived and compared to current lattice data. Our conclusions are in Sec. IV.

II. ELECTROMAGNETIC RADIATION FROM HADRONIC GAS

A. Dilepton and photon rates

In this section we review the spectral approach for the dilepton and photon production from a hadronic gas in thermal equilibrium [11,16,25]. The main advantage of the spectral function approach is that the calculation can be organized in a virial-like expansion and in principle all possible reaction channels can be included in the zero temperature spectral densities. The dilepton rate R, the number of dileptons produced per unit four volume, can be expressed using the current-current correlator as

$$\frac{dR}{d^4q} = \frac{-\alpha^2}{6\pi^3 q^2}\left(1 + \frac{2m_l^2}{q^2}\right)\left(1 - \frac{4m_l^2}{q^2}\right)^{1/2}\mathbf{W}(q), \quad (1)$$

where $\alpha = e^2/4\pi$ is the fine structure constant, $M \equiv \sqrt{q^2}$ is the dilepton invariant mass, m_l is the lepton mass and the un-ordered electromagnetic current-current correlator is given by [12,27]

$$\mathbf{W}(q) = \int d^4x\, e^{-iq\cdot x} \mathrm{Tr}[e^{-(\mathbf{H}-\mathbf{F})/T}\,\mathbf{J}^\mu(x)\mathbf{J}_\mu(0)]. \quad (2)$$

Here $\mathbf{H}$ is the hadronic Hamiltonian, $\mathbf{F}$ is the Helmholtz free energy, T is the temperature, and $e\mathbf{J}_\mu$ is the hadronic part of the electromagnetic current,

$$\mathbf{J}_\mu(x) = \sum_f \tilde{e}_f \, \overline{\mathbf{q}}_f \gamma_\mu \mathbf{q}_f(x) \tag{3}$$

with $\tilde{e}_f = (2/3, -1/3, -1/3)$. Note that we consider only three flavors which will be valid for the thermal electromagnetic emission below the charmonium peak.

Using the unordered correlator, Eq. (2), the number of real photons produced per unit volume and unit three-momentum can also be obtained as

$$\frac{q^0 dR}{d^3q} = -\frac{\alpha}{4\pi^2} \mathbf{W}(q) \tag{4}$$

with $q^2 = 0$. This equation with Eq. (1) enables us to link the *quasireal* virtual photon rate R^* with dielectron data in the low mass region below two pion threshold [1,28,29],

$$\frac{dR}{d^4q} = \frac{2\alpha}{3\pi M^2} \left(1 + \frac{2m_l^2}{M^2}\right) \left(1 - \frac{4m_l^2}{M^2}\right)^{1/2} \left(\frac{q^0 dR^*}{d^3q}\right). \tag{5}$$

In the limit of $M \to 0$, $R^* \approx R$.

Symmetry and spectral analysis allows us to re-express the unordered correlator in terms of the absorptive part of the Feynman correlator [30],

$$\mathbf{W}(q) = \frac{2}{e^{q^0/T}+1} \operatorname{Im}\mathbf{W}^F(q), \tag{6}$$

where the Feynman correlator with time-ordering (T^*) is given by

$$\mathbf{W}^F(q) = i \int d^4x \, e^{iq\cdot x} \operatorname{Tr}[e^{-(\mathbf{H}-\mathbf{F})/T} T^* \mathbf{J}^\mu(x)\mathbf{J}_\mu(0)]. \tag{7}$$

One can also obtain the retarded correlator from the Feynman correlator [30]

$$\operatorname{Im}\mathbf{W}^R(q) = \tanh(q^0/2T)\operatorname{Im}\mathbf{W}^F(q). \tag{8}$$

Using the retarded correlator one can obtain the electric conductivity from the linear response theory as we discuss later [21].

B. Mixing of vector and axial correlators in pionic gas

In Steele *et al.* [12] pion and nucleon contributions to the Feynman correlator were obtained within the context of a density expansion. For the heavy ion collisions where the net nucleon density is not negligible both pion and nucleon contributions are important [16]. However, for high energy collisions at RHIC and LHC, the pion contribution will dominate because the net baryon density of the fireball becomes negligible. In this work, we focus on the pion contributions. By taking the pion density as an expansion parameter, the pion contributions to the Feynman correlator

can be expressed as

$$\mathbf{W}^F(q) = \mathbf{W}_0^F(q) + \frac{1}{f_\pi^2} \int d\pi \, \mathbf{W}_\pi^F(q,k)$$
$$+ \frac{1}{2!} \frac{1}{f_\pi^4} \int d\pi_1 d\pi_2 \, \mathbf{W}_{\pi\pi}^F(q,k_1,k_2) + \cdots, \tag{9}$$

where

$$\mathbf{W}_0^F(q) = i \int d^4x \, e^{iq\cdot x} \langle 0|T^*\mathbf{J}^\mu(x)\mathbf{J}_\mu(0)|0\rangle,$$

$$\mathbf{W}_\pi^F(q,k) = if_\pi^2 \int d^4x \, e^{iq\cdot x} \langle \pi^a(k)|T^*\mathbf{J}^\mu(x)\mathbf{J}_\mu(0)|\pi^a(k)\rangle,$$

$$\mathbf{W}_{\pi\pi}^F(q,k_1,k_2) = if_\pi^4 \int d^4x \, e^{iq\cdot x} \langle \pi^a(k_1)\pi^b(k_2)|T^*\mathbf{J}^\mu(x)$$
$$\times \mathbf{J}_\mu(0)|\pi^a(k_1)\pi^b(k_2)\rangle, \tag{10}$$

and

$$\int d\pi = \int \frac{d^3k}{(2\pi)^3} \frac{n(E-\mu_\pi)}{2E} \tag{11}$$

with $E = \sqrt{k^2 + m_\pi^2}$ and $n(\omega) = 1/(e^{\omega/T} - 1)$. Note that the finite pion chemical potential μ_π and the isospin sum over index a and b are included.

The first contribution $\mathbf{W}_0^F$ in (10) is dominated by Π_V, the transverse part of the vector correlator $\langle 0|T^*\mathbf{VV}|0\rangle$, which can be fixed by the measured electroproduction data [13,25],

$$\operatorname{Im}\mathbf{W}_0^F = -3\,q^2\operatorname{Im}\Pi_V(q^2). \tag{12}$$

This term vanishes for real photons with $q^2 = 0$ because the hadronic gas in thermal equilibrium is stable against spontaneous photon emission. One pion contribution $\mathbf{W}_\pi^F$ can be represented by the measurable vacuum correlators using the chiral reduction formulas [11,12],

$$\operatorname{Im}\mathbf{W}_\pi^F(q,k) = 12\,q^2\operatorname{Im}\Pi_V(q^2)$$
$$- 6\,(k+q)^2\operatorname{Im}\Pi_A((k+q)^2) + (q \to -q)$$
$$+ 8\big((k\cdot q)^2 - m_\pi^2 q^2\big)\operatorname{Im}\Pi_V(q^2)$$
$$\times \operatorname{Re}\Delta_R(k+q) + (q \to -q), \tag{13}$$

where $\operatorname{Re}\Delta_R = \operatorname{PP}[1/(k^2 - m_\pi^2 + i\epsilon^2)]$ is the real part (principle value) of the retarded pion propagator and Π_A is the transverse parts of the axial correlator $\langle 0|AA|0\rangle$ which also can be fixed using experimental data [13,25]. The full expression for the two-pion contribution is more complicated [12,16] and the important contributions to $\operatorname{Im}\mathbf{W}_{\pi\pi}^F$ are summarized in Appendix A.

The mixing of vector and axial correlators as an indication of chiral symmetry restoration has been discussed in the literature in the limit of zero chemical potential and zero pion mass [24,25]. In this work we extend the discussion in the presence of finite pion chemical potential and pion mass. The pion density plays a major role for the mixing between the vector-axial correlators. In order to see the main idea of mixing, we focus on the contributions up to leading order in pion density. Firstly, if we take $k \to 0$ and $m_\pi \to 0$ before the integration over the pion momentum [24,25], one can have a
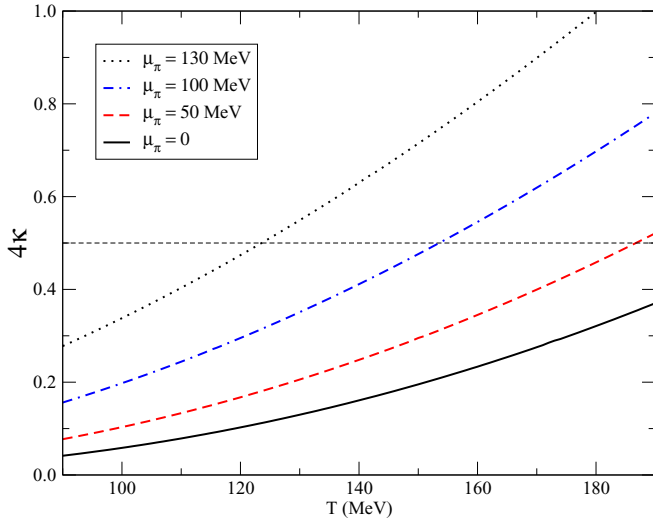
FIG. 1. (Color online) Pion density parameter κ vs temperature for different μ_π.

very schematic relation

$$\mathrm{Im}\mathbf{W}^F(q) \approx -3\,q^2[(1-4\kappa)\,\mathrm{Im}\Pi_V(q^2) + 4\kappa\,\mathrm{Im}\Pi_A(q^2)], \tag{14}$$

where κ is the dimensionless pion phase-space factor

$$\kappa = \frac{1}{f_\pi^2}\int d\pi \ . \tag{15}$$

The mixing is maximum for $\kappa \approx 1/8$, leading to the equal contribution from vector and axial correlators

$$\mathrm{Im}\mathbf{W}^F(q) \propto \mathrm{Im}(\Pi_V(q^2) + \Pi_A(q^2)). \tag{16}$$

In Fig. 1 we show the dependence of κ on the temperature for different pion chemical potentials μ_π. The vector-axial mixing (14) is enhanced at high temperature and/or higher μ_π as κ increases. With the full expression, since Eq. (13) depends on the pion momentum, the dependence on κ is not trivial. In Fig. 2 we show the partial contributions of Eqs. (12) and (13) to the imaginary part of the correlator, $-\mathrm{Im}\mathbf{W}^F$. In this figure one can clearly see that the one-pion contributions becomes significant as the pion chemical potential increases. The 50-50 mixing schematized in Eq. (16) is apparent qualitatively at $\mu_\pi = 100\,\mathrm{MeV}$ with which there is a large cancellation among the contributions with $\mathrm{Im}\Pi_V$. In Fig. 3 the dilepton rates are summarized with various pion chemical potentials. Due to the mixing, the low invariant mass dilepton production is enhanced while the ρ- around 0.78 GeV is reduced indicating the partial restoration of chiral symmetry.

C. Electric conductivity

To assess the electric conductivity from the hadronic gas we can use linear response and the Kubo-like formula for the spectral function

$$\rho_V(M,\vec{q}) = -\frac{2}{\tilde{\mathbf{e}}^2}\,\mathrm{Im}\mathbf{W}^R(M,\vec{q}), \tag{17}$$
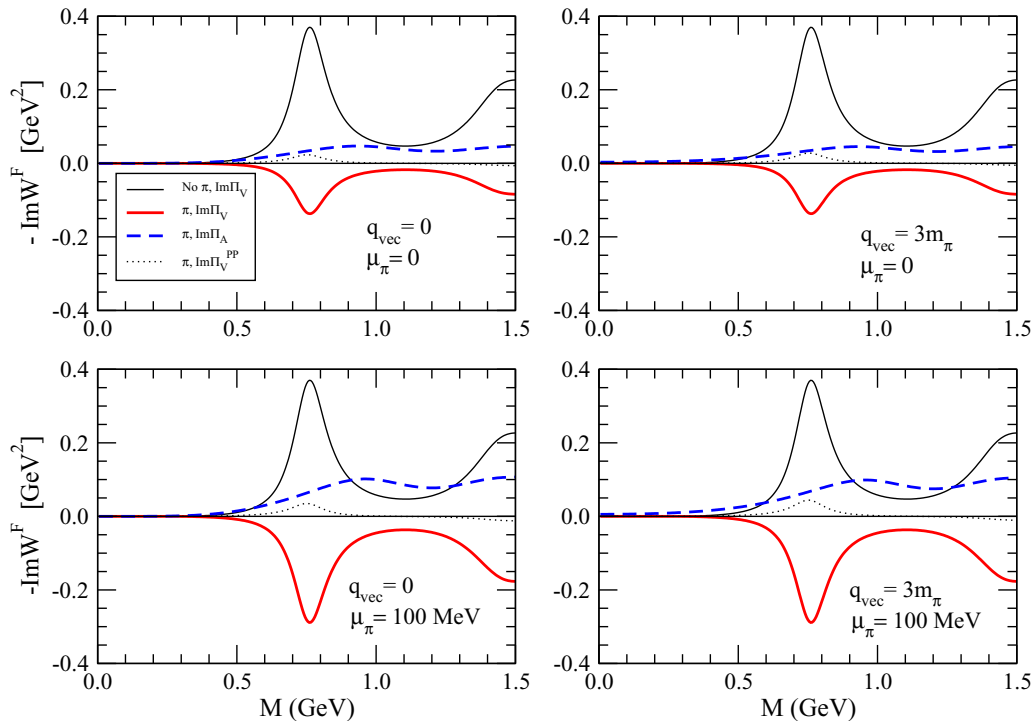
FIG. 2. (Color online) Partial contributions of Eqs. (12) and (13) to the imaginary part of the correlator $-\mathrm{Im}\mathbf{W}^F$ at $T = 190$ MeV for different $|\vec{q}|$ (q_{vec}) and μ_π. The thick black solid lines are the 0th order contribution without the pion. For the one pion contribution, labeled by π, the three lines in each figure correspond to the three lines in Eq. (13), respectively. PP represents the contribution from terms with the retarded pion propagator.
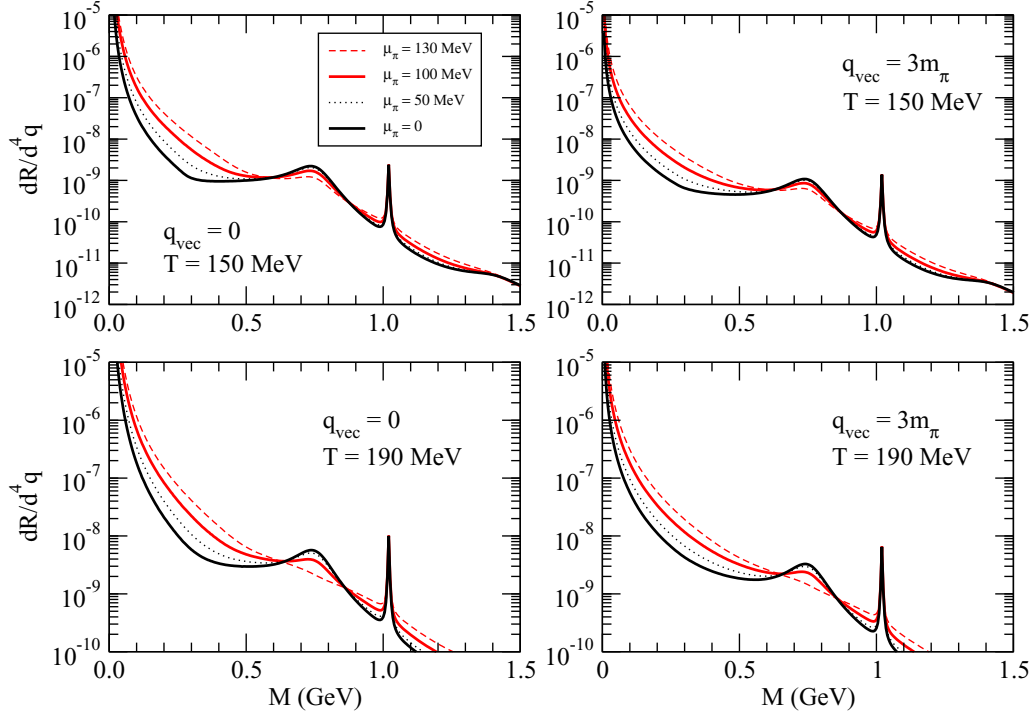
FIG. 3. (Color online) Dilepton rates for hadronic gas at $T = 150$ and 190 MeV with various $|\vec{q}|$ and μ_π.

where the sum of the squared flavor charge ratios $\tilde{e}^2 \equiv \sum_f \tilde{e}_f^2$ and $\rho_V = -\rho_{00} + \rho_{ii}$ [32]. In the $\vec{q} = 0$ limit

$$\rho_{ii}(M, \vec{0}) = \rho_V(M, \vec{0}) \tag{18}$$

because the time-like component $\rho_{00}(M, \vec{0})$ vanishes due to current conservation. In Fig. 4 we show ρ_V including terms up to κ^2 order for different values of $T, |\vec{q}|$, and μ_π. As μ_π increases, one can clearly see the mixing between the vector and axial correlator. The contribution from ϕ remains largely unaffected by the hadronic medium effects due to the OZI suppression rule. In Fig. 5 we summarize ρ_V / MT for various values of $|\vec{q}|$ at $T = 190$ MeV. In the left panel, one can see that the ρ_V is enhanced as the momentum $\vec{q}$ increases especially in the low invariant mass region. In the right panel, we plot the same quantity with and without the $A1$ meson. In the region of $M/T = 1 \sim 3$, the mixing between the vector and axial correlators are significant and the contribution of the $A1$ meson is very important.

The electric conductivity in unit of e^2 can be defined in the limit of $|\vec{q}|/M \to 0$ and $M \to 0$ as

$$\sigma_E = \lim_{M \to 0} \frac{\tilde{e}^2 \rho_{ii}(M, \vec{0})}{6M} = \lim_{M \to 0} \frac{-\text{Im} \mathbf{W}^R(M, \vec{0})}{3M}$$
$$= \lim_{M \to 0} \frac{-\text{Im} \mathbf{W}^F(M, \vec{0})}{6T}. \tag{19}$$

One can easily confirm that there is no contribution to σ_E from $\mathbf{W}_\pi^F$ because $\text{Im} \Pi_A(m_\pi^2) = 0$. In Fig. 5, from the curves with $|\vec{q}| = 0$, ρ_V / MT increases very rapidly as we decrease M. This behavior is caused by the pole of the retarded pion propagator in $\mathbf{W}_{\pi\pi}^F$ in the region $\epsilon \ll M$. In order to separate the finite contribution from the hadronic gas, one can take the

limit of $M/\epsilon \to 0$ for $\text{Re} \Delta_R(k + q)$,

$$\lim_{M/\epsilon \to 0} \text{Re} \Delta_R(k + q) = \lim_{M/\epsilon \to 0} \frac{M^2 + 2ME}{(M^2 + 2ME)^2 + \epsilon^4} \to 0. \tag{20}$$

In this limit, one can obtain a simple finite expression for the electric conductivity to order κ^2,

$$\frac{\sigma_E}{T} \approx \frac{(N_f^2 - 1)}{2T^2} \sum_{s=\pm} \int \frac{d\pi_1}{f_\pi^2} \frac{d\pi_2}{f_\pi^2} (k_1 + sk_2)^2$$
$$\times \text{Im} \Pi_V((k_1 + sk_2)^2). \tag{21}$$

In Fig. 6 the electric conductivities from a hadronic gas are compared with recent lattice results [21,31] and the lower bound [32] which are discussed in Sec. IIIB. The T and μ_π dependence of the hadronic gas is mainly caused by the pion distribution function. The hadron contribution to the electric conductivity is about an order of magnitude smaller than the reported lattice results [21,31] but comparable to the results of unitarized chiral perturbation [33].

For completeness, we note that to one-loop in ChPT the vector spectral function in Eq. (21) can be explicitly assessed. The result for the electric conductivity is

$$\frac{\sigma_E}{T} \approx \frac{(N_f^2 - 1)}{96\pi T^2} \sum_{s=\pm} \int \frac{d\pi_1}{f_\pi^2} \frac{d\pi_2}{f_\pi^2} \Theta\left((k_1 + sk_2)^2 - 4m_\pi^2\right)$$
$$\times (k_1 + sk_2)^2 \left(1 - \frac{4m_\pi^2}{(k_1 + sk_2)^2}\right)^{3/2} \tag{22}$$
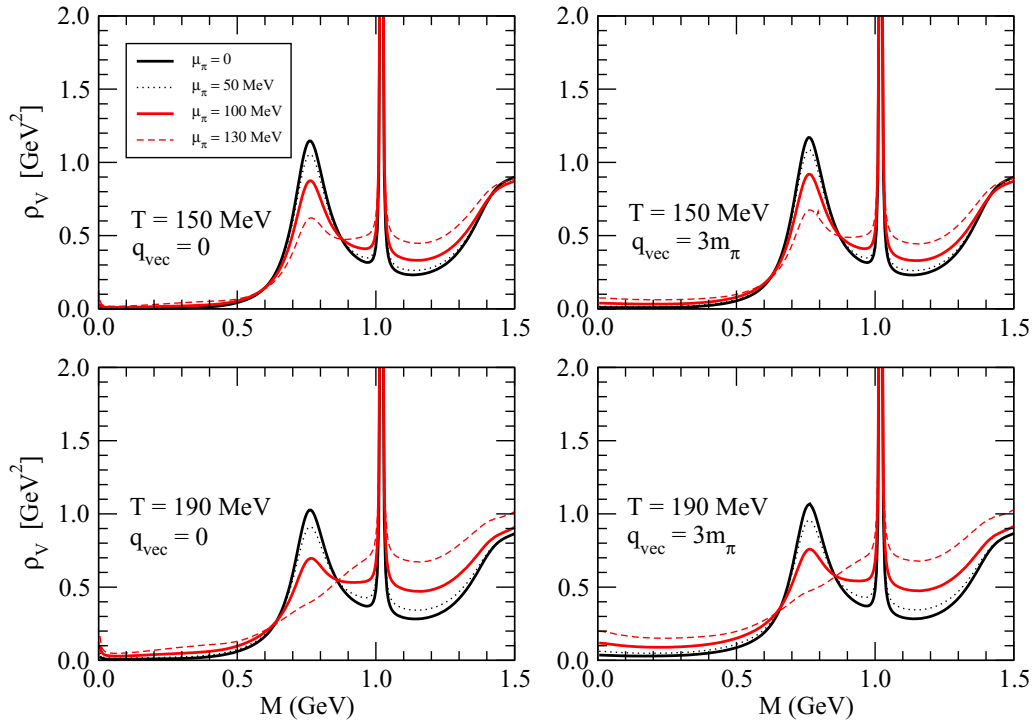
FIG. 4. (Color online) Spectral function ρ_V of the hadronic gas for $T = 150$ and 190 MeV with various $|\vec{q}|$ and μ_π.

which vanishes in the chiral limit as

$$\frac{\sigma_E}{T} \approx \frac{(N_f^2 - 1)T^4}{96\pi \, f_\pi^4} \, \mathbf{f}\left(\frac{m_\pi}{T}\right)$$

$$= \frac{(N_f^2 - 1)}{24\pi} \frac{\kappa^2 m_\pi^2}{T^2} + \mathcal{O}\left(\frac{m_\pi^3}{T^3}\right). \tag{23}$$

In the low temperature limit we have

$$\frac{\sigma_E}{T} \approx \frac{(N_f^2 - 1)m_\pi^6}{96\pi T^2 \, f_\pi^4} \, \mathbf{g}\left(\frac{T}{m_\pi}\right) \tag{24}$$

which is seen to vanish exponentially with the temperature since $\mathbf{g}(T/m_\pi) \propto e^{-2m_\pi/T}$.
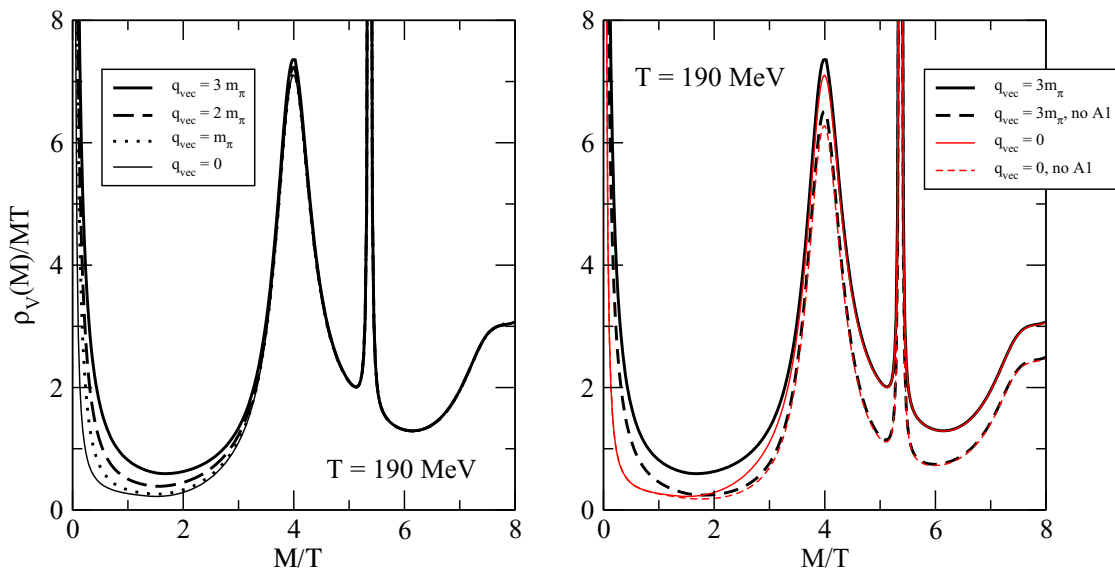
FIG. 5. (Color online) ρ_V/MT of the hadronic gas at $T = 190$ MeV and $\mu_\pi = 0$. The left panel shows the $|\vec{q}|$ dependence and the right panel shows the contribution of the $A1$ meson which is included in $\mathrm{Im}\Pi_A$.
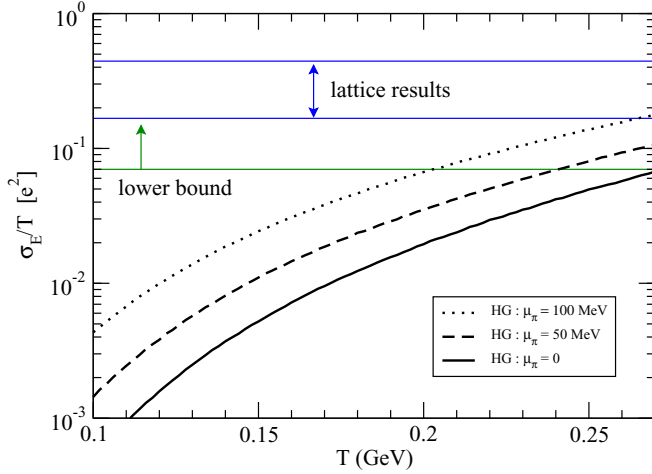
FIG. 6. (Color online) σ_E/T for the hadronic gas. The blue lines indicate the range of lattice results for two flavors [21,31] and the green line indicates the lower bound [32].

D. Quark number susceptibility

The electric conductivity in unit of e^2 can be tied with the flavor diffusion constant D_f through the identity [32]

$$\sigma_E = \chi_f \left[\left(\sum_{f=1}^{N_f} \tilde{e}_f \right)^2 \mathbf{D}_f^{\mathrm{S}} + \left(\sum_{f=1}^{N_f} \tilde{e}_f^2 \right) \mathbf{D}_f^{\mathrm{NS}} \right] \quad (25)$$

with $\mathbf{D}^{\mathrm{S,NS}}$ the singlet (S) and nonsinglet (NS) flavor diffusion constants and χ_f the flavor susceptibility

$$\chi_f = \frac{1}{TV_3} \langle \mathbf{Q}_f^2 \rangle \quad (26)$$

defined in terms of the conserved flavor charge

$$\mathbf{Q}_f = \int d\vec{x} \, J_f^0(0,\vec{x}). \quad (27)$$

Note that the singlet susceptibility vanishes for three flavors.

In the hadronic gas, the flavor susceptibility is better sought in terms of the fluctuations in the baryon number, isospin, and hypercharge density through the linear transformation

$$\begin{pmatrix} \mathbf{Q_u} \\ \mathbf{Q_d} \\ \mathbf{Q_s} \end{pmatrix} = \begin{pmatrix} 1 & 1 & \frac{1}{2} \\ 1 & -1 & \frac{1}{2} \\ 1 & 0 & -1 \end{pmatrix} \begin{pmatrix} \mathbf{Q^B} \\ \mathbf{Q^I} \\ \mathbf{Q^Y} \end{pmatrix}, \quad (28)$$

where

$$\mathbf{Q^B} = \int d\vec{x} \, q^\dagger \frac{\mathbf{1}}{3} q = \int d\vec{x} \, \frac{1}{3}(u^\dagger u + d^\dagger d + s^\dagger s),$$

$$\mathbf{Q^I} = \int d\vec{x} \, q^\dagger \frac{\lambda^3}{2} q = \int d\vec{x} \, \frac{1}{2}(u^\dagger u - d^\dagger d),$$

$$\mathbf{Q^Y} = \int d\vec{x} \, q^\dagger \frac{\lambda^8}{\sqrt{3}} q = \int d\vec{x} \, \frac{1}{3}(u^\dagger u + d^\dagger d - 2s^\dagger s).$$

$$(29)$$

Here $\mathbf{Q^B}$, $\mathbf{Q^I}$, and $\mathbf{Q^Y}$ correspond to the baryon number, isospin, and hypercharge operators, respectively.

In the pionic gas which we are considering in this work, the flavor susceptibility becomes flavor-dependent because the SU(3) symmetry is partially broken due to the explicit mass differences in the meson octet,

$$\begin{pmatrix} \chi_u \\ \chi_d \\ \chi_s \end{pmatrix} = \frac{1}{TV_3} \begin{pmatrix} 1 & 1 & \frac{1}{4} \\ 1 & 1 & \frac{1}{4} \\ 1 & 0 & 1 \end{pmatrix} \begin{pmatrix} \langle (\mathbf{Q^B})^2 \rangle \\ \langle (\mathbf{Q^I})^2 \rangle \\ \langle (\mathbf{Q^Y})^2 \rangle \end{pmatrix}, \quad (30)$$

where $\langle (\mathbf{Q^B})^2 \rangle = \langle (\mathbf{Q^Y})^2 \rangle = 0$ and $\chi_s = 0$ for the pionic gas.

Using the pion density expansion we have

$$\langle (\mathbf{Q^I})^2 \rangle = \langle (\mathbf{Q^I})^2 \rangle_\pi + \langle (\mathbf{Q^I})^2 \rangle_{\pi\pi} + \cdots \quad (31)$$

with

$$\langle (\mathbf{Q^I})^2 \rangle_\pi = \int d\pi \, \langle \pi^a(k) | (\mathbf{Q^I})^2 | \pi^a(k) \rangle$$

$$= \mathbf{I}_\pi^2 V_3 N_\pi \int \frac{d^3 k}{(2\pi)^3} n(E - \mu_\pi) \quad (32)$$

and

$$\langle (\mathbf{Q^I})^2 \rangle_{\pi\pi} = \frac{1}{2!} \int d\pi^a(k_1) d\pi^b(k_2) \left[\langle \pi^a(k_1) | (\mathbf{Q^I})^2 | \pi^b(k_2) \rangle \right.$$

$$\times \langle \pi^b(k_2) | \pi^a(k_1) \rangle + (a,k_1 \leftrightarrow b,k_2) \right]$$

$$+ \frac{1}{2!} \int d\pi^a(k_1) d\pi^b(k_2) \, \mathrm{Im} \langle \pi^a(k_1) \pi^b(k_2) |$$

$$\times (\mathbf{S} - \mathbf{1}) (\mathbf{Q^I})^2 | \pi^a(k_1) \pi^b(k_2) \rangle, \quad (33)$$

where $\mathbf{I}_\pi^2 = 2$, $N_\pi = 3$, $\langle \pi^b(k_2) | \pi^a(k_1) \rangle = \delta^{ab}(2\pi)^3 \, 2E(k_1) \delta^3(k_2 - k_1)$, and $(2\pi)^3 \delta^3(\vec{0}) = V_3$.

The first exchange but disconnected contribution is shown separately. The connected contribution involves the full S-matrix after using Eq. (6). The result is the on-shell and forward $\pi\pi$ scattering amplitude $\mathcal{T}_{\pi\pi}$. The result is

$$\langle (\mathbf{Q^I})^2 \rangle_{\pi\pi} = \frac{2\mathbf{I}_\pi^2}{2!} V_3 N_\pi \int \frac{d^3 k}{(2\pi)^3} [n(E - \mu_\pi)]^2$$

$$+ \frac{2\mathbf{I}_\pi^2}{2!} \int d\pi^a(k_1) d\pi^b(k_2) (2\pi)^4 \delta^4$$

$$\times (k_1 + k_2 - (k_1 + k_2)) \, \mathrm{Re} \mathcal{T}_{\pi\pi}^{ab,ab}(k_1,k_2), \quad (34)$$

where $(2\pi)^4 \delta^4(0) \equiv V_3/T$. Thus

$$\chi_{u,d} = \frac{1}{TV_3} \langle (\mathbf{Q^I})^2 \rangle$$

$$\approx \mathbf{I}_\pi^2 \left[\frac{N_\pi}{T} \int \frac{d^3 k}{(2\pi)^3} n(1+n) \right.$$

$$+ \frac{1}{T^2} \int \frac{d^3 k_1}{(2\pi)^3} \frac{n_1}{2E_1} \frac{d^3 k_2}{(2\pi)^3} \frac{n_2}{2E_2} \, \mathrm{Re} \mathcal{T}_{\pi\pi}(s,t,u) \right] \quad (35)$$

with the Mandelstam variables $s = (k_1 + k_2)^2$, $t = (k_1 - k_2)^2$, $u = 0$. To leading order in ChPT the $\pi\pi$ scattering amplitude is given by the Weinberg term. Specifically,

$$\chi_{u,d} \approx \mathbf{I}_\pi^2 \left[\frac{N_\pi}{T} \int \frac{d^3 k}{(2\pi)^3} n(1+n) - \kappa^2 N_\pi(N_\pi - 2) \frac{m_\pi^2 f_\pi^2}{T^2} \right], \quad (36)$$
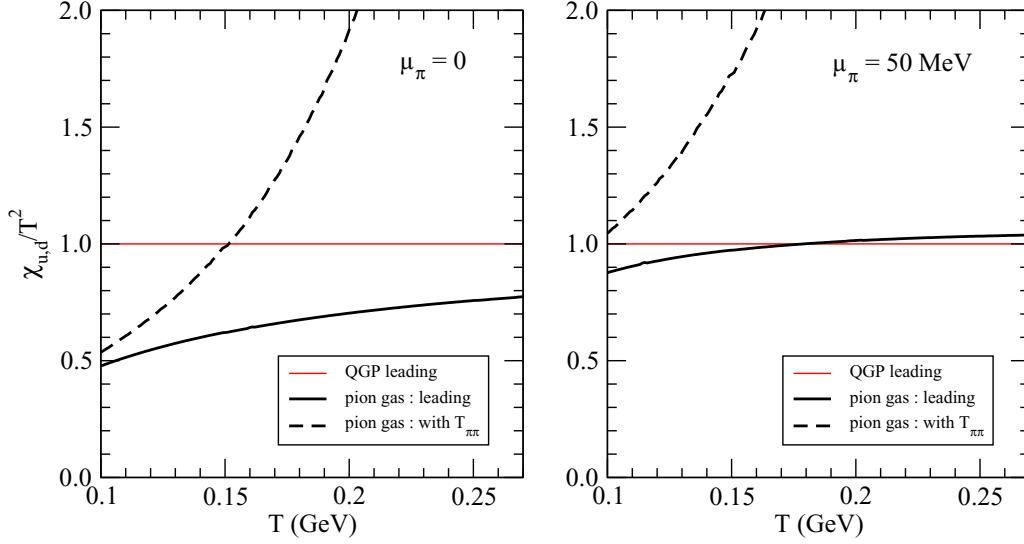
FIG. 7. (Color online) Flavor susceptibilities of the pionic gas. Red thin solid line corresponds to the leading QGP result $\chi_{u,d}/T^2 = N_c/3$. The black thick solid line corresponds to the leading contribution with $\int d^3k \, n(1+n)$ and the black thick dashed line corresponds to the susceptibilities with $\mathcal{T}_{\pi\pi}$ as in Appendix B.

where the tree level $\pi\pi$ contribution is seen to be negative and vanishing in the chiral limit. The full result for the second order correction using the chirally reduced forward $\pi\pi$-scattering amplitude is given in Appendix B in terms of the pion scalar and vector form factors and vacuum correlators [34,35]. In Fig. 7, the flavor susceptibilities of the pionic gas are summarized. At low temperature the leading contribution dominates compared to the $\mathcal{T}_{\pi\pi}$ contribution. However, as the temperature increases, the $\mathcal{T}_{\pi\pi}$ contribution dominates due to the extra T^2 dependence compared to the leading contribution. The increase in the two pion correlations around the transition temperature is expected. While the diluteness factor $4\kappa \approx 0.2$ in this temperature range (see Fig. 1) is small, the forward two pion scattering amplitude is large due to the threshold enhancement in the vector channel. Such kinematical effects are expected in the hadronic organization of the thermal averages. They do not invalidate the κ-expansion. Indeed, we do not expect further three pion etc. kinematical enhancements in the bulk susceptibilities. We recall that the two pion contribution in Eq. (9) is very important for the dilepton rate enhancement, especially at very low invariant mass M. Note that there are finite external four-momentum ($q^2 = M^2$) for the dilepton rate which suppress the two pion contribution via vector and axial correlators for large invariant mass M. In Fig. 7 the leading QGP contribution is given by the red thin lines. Higher order corrections to the sQGP susceptibility are discussed later in Sec. IIIC.

III. ELECTROMAGNETIC RADIATION FROM A STRONGLY INTERACTING QUARK-GLUON PLASMA

A. Nonperturbative thermal condensates

There has been great progress in the calculation of the perturbative photon emission rates in a weakly coupled QCD plasma at asymptotic temperatures [36]. The leading contribution to the photon rates comes from two-loop diagrams

corresponding to the process $q + \overline{q} \to \gamma + g$ and Compton $g + q(\overline{q}) \to q(\overline{q}) + \gamma$ processes. However these rates are plagued with collinear singularities. Instead, a complete leading order photon emission requires the inclusion of collinear bremsstrahlung and inelastic pair annihilations and their subsequent suppression through the LPM effect [36]. The extension of these calculations to the dilepton rates at asymptotic temperatures is not available.

At current collider energies the QCD plasma is strongly coupled or sQGP. The perturbative calculations are at best suggestive and a more nonperturbative framework for time-like processes is needed to separate the hard partonic physics which is perturbative from the soft partonic physics which is not. A useful framework for this approach is the one advocated long ago by Hansson and one of us [18] whereby the vacuum OPE expansion for current-current correlators is reordered at high temperature to account for the soft thermal gluon corrections through pertinent electric and magnetic condensates much in the spirit of the QCD sum rules in the nonperturbative vacuum. Its application to thermal dileptons was already used in [19].

The approach works as follows: The leading order contribution to the retarded current-current correlator, Eq. (8), is the Born $q\bar{q}$ annihilation term,

$$\text{Im} \, \mathbf{W}_0^R(q) = \frac{N_c \tilde{\mathbf{e}}^2}{4\pi} q^2 \left[1 + \frac{2T}{|\vec{q}|} \ln \left(\frac{n_+}{n_-} \right) \right], \quad (37)$$

where N_c is the number of colors and $n_\pm$ the quark occupation numbers

$$n_\pm = \frac{1}{e^{(q_0 \pm |\vec{q}|)/2T} + 1}. \quad (38)$$

Note that this contribution vanishes at the photon point, $q^2 = 0$, due to energy momentum conservation [19]. The sQGP around the critical temperature is expected to display non-perturbative effects in the form of soft gluons, which can be characterized by thermal condensates of gauge-invariant
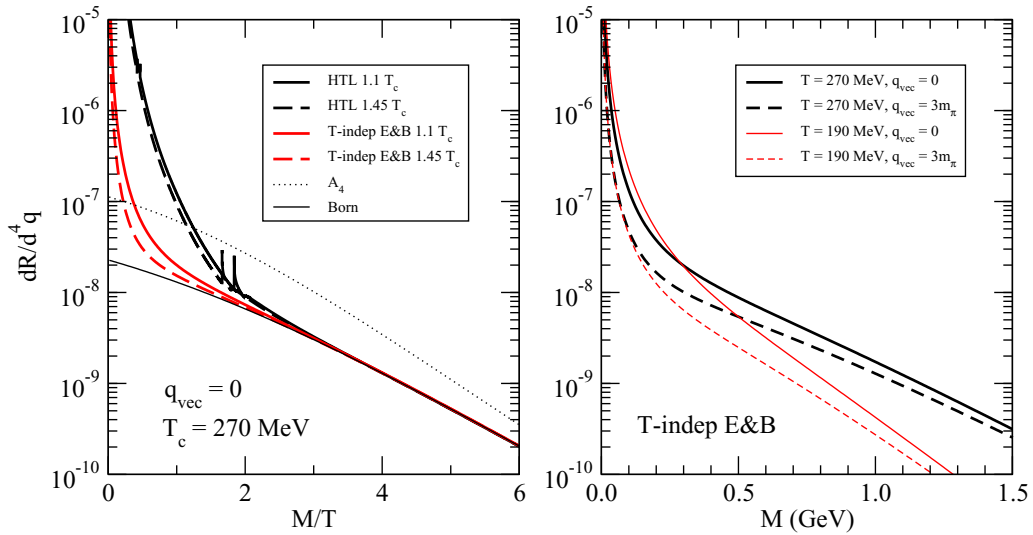
FIG. 8. (Color online) Thermal dileptons. Left panel: sQGP and HTL. Right panel: T and $|\vec{q}|$ dependence of the sQGP. T-independent $\langle B^2 \rangle$ and $\langle E^2 \rangle$ in Eq. (41) are used for the sQGP.

operators of leading mass dimensions such as $\langle A_4^2 \rangle$, $\langle E^2 \rangle$, and $\langle B^2 \rangle$. Their contributions to the dilepton emissivities in leading order are [18,19]

$$\text{Im}\,\mathbf{W}_2^R(q) = \frac{N_c \tilde{\mathbf{e}}^2}{4\pi} q^2 \left\langle \frac{\alpha_s}{\pi} A_4^2 \right\rangle \left(\frac{4\pi^2}{T|\vec{q}|} \right) (n_+(1-n_+)$$
$$- n_-(1-n_-)) \tag{39}$$

and

$$\text{Im}\,\mathbf{W}_4^R(q) = \frac{N_c \tilde{\mathbf{e}}^2}{4\pi} \left[-\frac{1}{6}\left\langle \frac{\alpha_s}{\pi} E^2 \right\rangle + \frac{1}{3}\left\langle \frac{\alpha_s}{\pi} B^2 \right\rangle \right] \left(\frac{4\pi^2}{T|\vec{q}|} \right)$$
$$\times (n_+(1-n_+) - n_-(1-n_-)). \tag{40}$$

Across the phase transition temperature T_c which is first order for pure gluodynamics, the electric and magnetic condensates fall by about half their value in the QCD vacuum in the

temperature range $(1-3)T_c$, and remain about constant in this range [37]. Thus for $T_c < T < 3T_c$ in Euclidean signature this translates to

$$\langle \alpha_s B^2 \rangle \approx \langle \alpha_s E^2 \rangle \approx \frac{1}{2} \times \frac{1}{4} \langle \alpha_s G^2 \rangle_0 \tag{41}$$

in terms of the vacuum gluon condensate [37]. We use the updated value of the gluon condensate $\langle \alpha_s G^2 \rangle_0 = 0.068$ GeV^4 [38]. In Fig. 8, the dilepton rates from the sQGP are summarized for various temperatures and momenta $q = |\vec{q}|$. In order to check the contribution from $\langle A_4^2 \rangle$, we used $\langle \frac{\alpha_s}{\pi} A_4^2 \rangle / T^2 \approx 0.4$ for the plot [19]. The presence of $\langle A_4^2 \rangle$ appears to be ruled out by a comparison to the recent lattice data [23]. In the left panel, for the comparison, we also plot the contribution form the HTL (hard thermal loop) [39]. One can see that the enhancement in the low mass region mainly comes from the $\langle E^2 \rangle$ and $\langle B^2 \rangle$ contributions even though
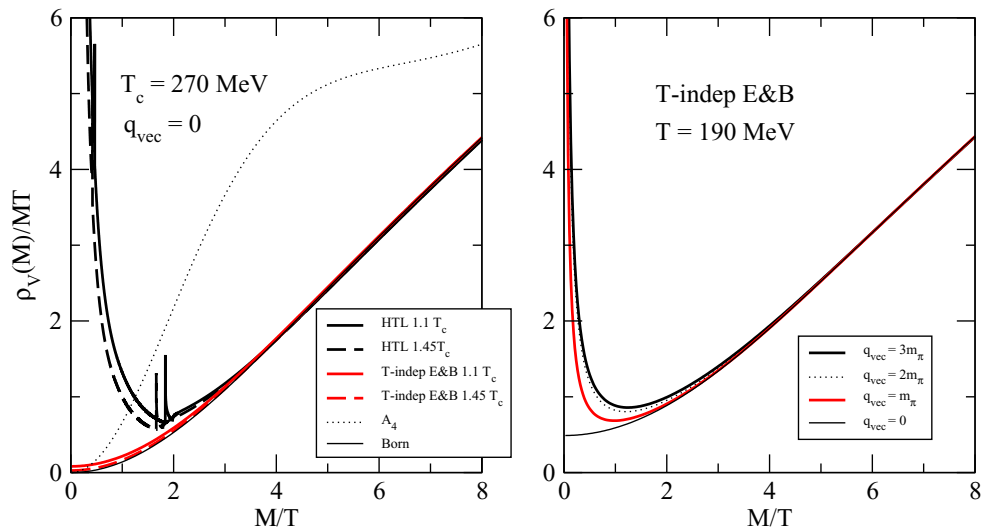
FIG. 9. (Color online) Vector spectral density. Left panel: comparison between sQGP and HTL results. Right panel: $|\vec{q}|$ dependence of sQGP. T-independent $\langle B^2 \rangle$ and $\langle E^2 \rangle$ in Eq. (41) are used for sQGP.

they are smaller than the HTL results. In Braaten *et al.* [39], power counting is taken into account even for the Fermi-Dirac distribution function, which is valid in the soft energy region. However, in this work, we kept the full expression of the Fermi-Dirac distribution function in the HTL calculation in order to compare with other results. In the right panel of Fig. 8, the temperature and momentum dependence of the sQGP rate are summarized. By comparing results for $T = 190$ MeV in Figs. 3 and 8, one can see that the hadronic contributions are significantly higher than the sQGP contributions in the low mass region below 0.1 MeV as the chemical potential increases.

In Fig. 9 we plot the vector spectral densities, which can be compared with the results from the hadronic gas summarized in Fig. 5. In the left panel of Fig. 9 we compare the results at two high temperatures of $1.1 T_c$ and $1.45 T_c$ with the critical temperature for quenched calculation $T_c = 270$ MeV [21]. The leading Born contribution is compared to the contribution including the soft gluon condensates as well as the hard thermal loops [39,40]. In the right panel the same spectral densities are shown for different momenta $\vec{q} \neq 0$ at $T = 190$ MeV. With finite thermal condensate $\langle E^2 \rangle$ and $\langle B^2 \rangle$ contribution, the ρ_V / MT increases as the momentum increases for any given M, especially in the low mass region the enhancement is significant. A comparison with recent lattice results confirms the important of the thermal condensate in the sQGP [23].

B. Electric conductivity

The electric conductivity σ_E at high temperature plays an important role in recent developments related to the chiral magnetic effects in the early stage of the sQGP. Our condensate corrections to the Euclidean spectral function allow us to make an estimate of σ_E across the transition region by tying it to the spectral function in the zero mass limit as in Eq. (19). The only drawback is that the reorganized OPE expansion at high temperature [18,19] is an expansion in $\mathbf{M}^2 / |\vec{q}|^2 < 1$, with $\mathbf{M}$ the soft scale in the matrix element which is typically the magnetic scale. The extrapolation of the leading operator corrections to $|\vec{q}| \to 0$ while finite calls for corrections of order 1 from the higher operator insertions. This notwithstanding, an estimate of the electric conductivity is set by the leading dimension-4 operators at high temperature

$$\sigma_E \approx \frac{\pi N_c \tilde{\mathbf{e}}^2}{48 T^3} \left(-\frac{1}{6} \left\langle \frac{\alpha_s}{\pi} E^2 \right\rangle + \frac{1}{3} \left\langle \frac{\alpha_s}{\pi} B^2 \right\rangle \right). \quad (42)$$

Lattice results show that σ_E / T is weakly dependent on the temperature and the value lies in the range $0.3 < \sigma_E / \tilde{\mathbf{e}}^2 T < 0.8$ [21,31]. Recent analysis with PHENIX data gives slightly larger value $0.5 < \sigma_E / T < 1.1$ [41]. The temperature dependence of σ_E / T has been also reported in the literature [42–46], in which σ_E / T increases as the temperature increases above T_c. Burnier and Laine [32] got a lower bound for the electric conductivity, or $\sigma_E / T \geqslant 0.07$, which is significantly smaller than previous leading-order weak-coupling expansion results [47,48].

In Fig. 10, we plot the electric conductivity for the sQGP with constant $\langle B^2 \rangle$ and $\langle E^2 \rangle$. Our sQGP results with constant $\langle B^2 \rangle$ and $\langle E^2 \rangle$ are much smaller than the lattice
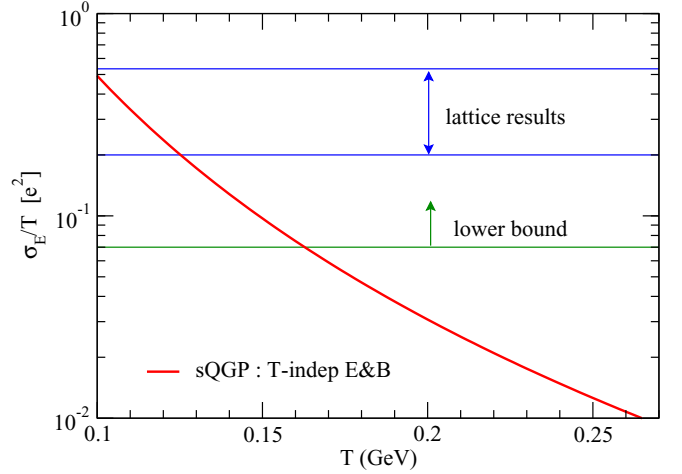
FIG. 10. (Color online) σ_E / T for sQGP. The blue lines indicate the range of lattice results for three flavors [21,31] and the green line indicates the lower bound [32].

estimates [21,31]. At large temperatures the electric and magnetic condensates are T dependent with $\langle B^2 \rangle \approx \langle E^2 \rangle \approx (b \pi^2 / 20) \times T^4$ and $b \approx 1$–1.2 [49]. On the other hand, a fit to the currently reported lattice conductivities suggest

$$\langle \alpha_s E^2 \rangle \approx \langle \alpha_s B^2 \rangle \approx \frac{288}{N_c} \left\langle \frac{\sigma_E}{\tilde{\mathbf{e}}^2 T} \right\rangle T^4 \approx 48 \, T^4 \quad (43)$$

with $\langle \sigma_E / \tilde{\mathbf{e}}^2 T \rangle \sim 0.5$ at about the mean value of the lattice results [21,31].

Therefore, the electric conductivity as well as the comparison with lattice results appear to rule out the sQGP approach with T-independent condensates $\langle B^2 \rangle$ and $\langle E^2 \rangle$. In Fig. 11, we plot the dilepton rate and spectral density with T-dependent condensates. In comparison with Figs. 8 and 9 one can see the significant enhancement in the low mass region. The Born term dominates in the high mass region and the results are rather insensitive to the details of the thermal condensates.

C. Flavor diffusion constant

The partonic flavor susceptibility can be sought along the same arguments as those developed for the hadronic parts, using the QCD Hamiltonian at high temperature, as summarized in Appendix C. However, in this work, instead of calculating the contributions of T_{qq} explicitly, we compare our pionic gas results in Fig. 7 with the recent lattice results [50]. Lattice results indicate that the quark susceptibilities drop by about $15 \sim 25$ % compared to the Stefan-Boltzmann limit near the phase transition temperature. The leading contribution from the pionic gas is close to the lattice results. However, as noted earlier, the higher order corrections from $\mathcal{T}_{\pi\pi}$ become significant in the critical temperature region and the perturbative treatment is not valid.

Since $\mathbf{D}_f^{NS} / \mathbf{D}_f^S \sim N_c$ this makes the nonsinglet contribution dominant for $N_c = 3$ assumed large. Thus, with $\chi_f = (N_c / 3) T^2$,

$$T \mathbf{D}_f^{NS} \approx \frac{T \sigma_E}{\tilde{\mathbf{e}}^2 \chi_f} \approx \frac{3}{N_c} \frac{\sigma_E}{T \tilde{\mathbf{e}}^2} \approx \frac{1}{2}, \quad (44)$$
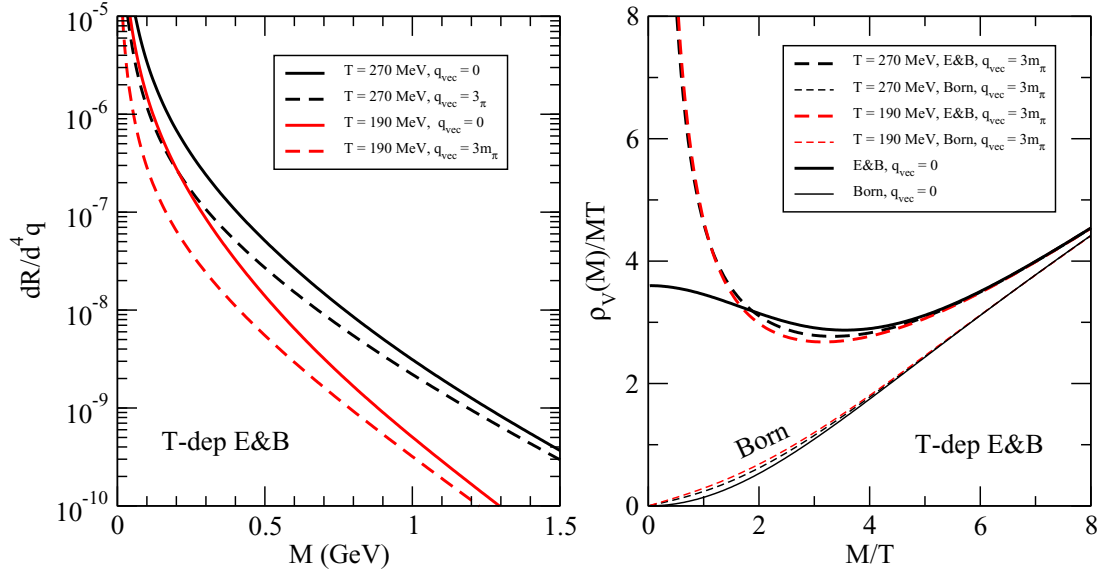
FIG. 11. (Color online) Dileptons rates and spectral function from the sQGP with T-dependent $\langle E^2 \rangle$ and $\langle B^2 \rangle$ in Eq. (43).

where in the last estimate we used the central value of the lattice estimate for the electric conductivity [21,31], across the transition temperature. Note that this value lies between the results from the AdS/CFT [51] and the phenomenological approach [52]. In the intermediate regime of temperatures $(1 - 3) T_c$ the light flavor quarks carry a thermal mass of the order of the Matsubara mass $m_T \approx \pi T > T$ making the light flavors somehow heavy in comparison to the typical thermal excitations. In the large N_c limit and using the Einstein relation we can estimate the drag η_f on the light quarks in the transition region [53,54]

$$\frac{\eta_f}{T} \approx \frac{1}{m_T \mathbf{D}_f^{NS}} \approx \frac{N_c T}{3 m_T} \frac{\tilde{\mathbf{e}}^2 T}{\sigma_E} \ . \tag{45}$$

If we use the central value of the lattice result for the electric conductivity, then $\eta_f/T \approx 2/\pi$ across the transition temperature. This drag quantifies the amount of Brownian motion for the light flavors in the sQGP.

IV. CONCLUSIONS

Our hadronic rates are based on the use of spectral functions. Unlike kinetic processes whereby each emission is associated with particular Feynman diagrams, our spectral analysis enforces all the constraints of broken chiral symmetry, and through the spectral weights accounts for tails of resonances. It does not rely on any effective Lagrangian, and therefore does not suffer the drawback of a strong interaction expansion and the ambiguities associated to hadronic form factors. However, it is limited by a reorganization of the leptonic emissivities around the resonance gas model to leading order, with one- and two-pion final re-scattering in the initial states. Carrying out the expansion to three-pion rescattering in the initial state is formidable.

We have shown that the mixing between the vector and axial correlators becomes more significant with increasing pion chemical potentials indicating the partial restoration of chiral symmetry. This mixing enhances the dilepton rate significantly at low invariant mass. The evolved rates account well for the dilepton emissivities reported by the SPS (see [6] and references therein). Although the inclusion of baryons, should improve slightly the fit, we are confident that our organization of the dilepton emissivities through the virial expansion works at collider energies.

Since our photon rates fit reasonably well the low mass photon spectra at collider energies [16] we can use them to extract both the electric conductivity and the flavor susceptibility constant in the hadronic phase. We have found that the electric conductivity at $T \approx m_\pi$ is substantially smaller than the currently reported lattice conductivities. While we have not included the contributions of order κ^3 and higher, we believe that our chiral expansion provides a sound starting estimate based on the strictures of spontaneously broken chiral symmetry. The flavor susceptibility in the correlated hadronic gas is reasonably close to the reported lattice results at the transition temperature.

We have provided first principle estimates of the corrections to the electromagnetic emissivities in the partonic phase and near the transition temperature using the high temperature QCD sum rule method [18,19], whereby the effects of soft gluons are retained in the form of gluonic matrix elements. A reasonable account of the electric conductivities reported on the lattice at high temperature is reproduced with temperature dependent condensates.

The approach we have discussed can be extended to most transport coefficients in QCD both below and above the transition temperature. It is well motivated by the structures of chiral symmetry below the transition temperature, and by a reorganization of the OPE expansion at high temperature. The dual nature of the interacting resonance gas model near the transition temperature with its high-temperature partonic description, provides us with an interesting nonperturbative tool for computing the transport parameters of QCD matter near equilibrium.

APPENDIX A: TWO-PION CONTRIBUTION $\mathbf{W}_{\pi\pi}^F$

The two-pion contribution $\mathbf{W}_{\pi\pi}^F$ which is important both for the rate and the electric conductivity is more involved [12,26]. We summarize the dominant contributions [16]

$$
\begin{aligned}
\frac{1}{f_\pi^4}&\mathrm{Im}\mathbf{W}_{\pi\pi}^F(q,k_1,k_2)\\
&= \frac{2}{f_\pi^2}[g_{\mu\nu}-(2k_1+q)_\mu k_{1\nu}\mathrm{Re}\Delta_R(k_1+q)]\mathrm{Im}\mathcal{T}_{\pi\gamma}^{\mu\nu}(q,k_2)\\
&+(q\to-q)+(k_1\to-k_1)+(q,k_1\to-q,-k_1)\\
&+\frac{1}{f_\pi^2}k_1^\mu(2k_1+q)^\nu\mathrm{Re}\Delta_R(k_1+q)\epsilon^{a3e}\epsilon^{e3g}\mathrm{Im}\mathcal{B}_{\mu\nu}^{ag}(k_1,k_2)\\
&-\frac{1}{f_\pi^2}[g^{\mu\nu}-(k_1+q)^\mu(2k_1+q)^\nu\mathrm{Re}\Delta_R(k_1+q)]\\
&\times\epsilon^{a3e}\epsilon^{a3f}\mathrm{Im}\mathcal{B}_{\mu\nu}^{ef}(k_1+q,k_2)\\
&+\frac{1}{f_\pi^2}(k_1+q)^\mu(k_1+q)^\nu(2k_1+q)^2[\mathrm{Re}\Delta_R(k_1+q)]^2\\
&\times\epsilon^{a3e}\epsilon^{a3f}\mathrm{Im}\mathcal{B}_{\mu\nu}^{ef}(k_1+q,k_2)+(k_1\to-k_1).
\end{aligned}
\tag{A1}
$$

The pion-spin averaged $\pi\gamma$ forward scattering amplitude $\mathrm{Im}\mathcal{T}_{\pi\gamma}$ is given as [26]

$$
\begin{aligned}
\mathrm{Im}\mathcal{T}_{\pi\gamma}^{\mu\nu}(q,k) &= \frac{2}{3f_\pi^2}(2k^\mu+q^\mu)(-q^2k^\nu+k\cdot q\,q^\nu)\\
&\times\mathrm{Re}\Delta_R(k+q)\mathrm{Im}\Pi_V(q^2)\\
&+(q\to-q)+(k\to-k)+(q,k\to-q,-k)\\
&+\frac{4}{3f_\pi^2}(g^{\mu\nu}q^2-q^\mu q^\nu)\mathrm{Im}\Pi_V(q^2)\\
&-\frac{2}{3f_\pi^2}(g^{\mu\nu}(k+q)^2-(k+q)^\mu(k+q)^\nu)\\
&\times\mathrm{Im}\Pi_A((k+q)^2)\\
&+(k\to-k),
\end{aligned}
\tag{A2}
$$

and the contribution $\mathcal{B}$ reads [16,26]

$$
\begin{aligned}
\mathrm{Im}\mathcal{B}_{\mu\nu}^{ef}&(k_1,k_2)\\
&= \frac{2}{f_\pi^2}\delta^{ef}[g_{\mu\nu}(k_1+k_2)^2-(k_1+k_2)_\mu(k_1+k_2)_\nu]\\
&\times\mathrm{Im}\Pi_V((k_1+k_2)^2)
\end{aligned}
$$

$$
+(k_2\to-k_2)-\frac{4}{f_\pi^2}\delta^{ef}\left[g_{\mu\nu}k_1^2-k_{1\mu}k_{1\nu}\right]\mathrm{Im}\Pi_A\left(k_1^2\right).
\tag{A3}
$$

All additional spectral contributions to $\mathbf{W}_{\pi\pi}^F$ are thoroughly discussed in [12,26]. Their contribution to the photon and dilepton emissivities in the low and intermediate mass range is negligible.

APPENDIX B: $\pi\pi$ SCATTERING AMPLITUDE

Here we summarize the $\pi\pi$ scattering amplitudes which are relevant to the flavor susceptibility as [34,35]

$$
\begin{aligned}
\mathcal{T}_{\pi\pi}(s,t,u) &\equiv \sum_{a=d,b=c}\mathcal{T}_{\pi\pi}(p_2d,k_2b\leftarrow k_1a,p_1c)|_{p_2=k_1,p_1=k_2}\\
&= \mathcal{T}_{\mathrm{tree}}(s,t,u)+\mathcal{T}_{\mathrm{vector}}(s,t,u)+\mathcal{T}_{\mathrm{scalar}}(s,t,u)\\
&+\mathcal{T}_{\mathrm{rest}}(s,t,u)
\end{aligned}
\tag{B1}
$$

with Mandelstam variables

$$
\begin{aligned}
s &= (k_1+p_1)^2=(k_2+p_2)^2,\\
t &= (k_1-k_2)^2=(p_1-p_2)^2,\\
u &= (k_1-p_2)^2=(p_1-k_2)^2.
\end{aligned}
\tag{B2}
$$

For the contribution of thermal pions to the flavor susceptibility, $\delta^{ad}\delta^4(k_1-p_2)$, $\delta^{bc}\delta^4(p_1-k_2)$, and $u=0$ are implicitly considered and the identity $s+t+u=4m_\pi^2$ is used. The Weinberg tree contribution to the scattering amplitude can be reduced to a constant value as

$$
\begin{aligned}
\mathcal{T}_{\mathrm{tree}} &= \sum_{a=d,b=c}\left[\frac{1}{f_\pi^2}(s-m_\pi^2)\delta^{ac}\delta^{bd}+\frac{1}{f_\pi^2}(t-m_\pi^2)\delta^{ab}\delta^{cd}\right.\\
&\left.+\frac{1}{f_\pi^2}(u-m_\pi^2)\delta^{ad}\delta^{bc}\right]\\
&\Rightarrow N_\pi(2-N_\pi)\frac{m_\pi^2}{f_\pi^2}.
\end{aligned}
\tag{B3}
$$

The vector contribution to one-loop order can be represented as

$$
\begin{aligned}
\mathcal{T}_{\mathrm{vector}} &= \sum_{a=d,b=c}\left[\epsilon^{ace}\epsilon^{dbe}(u-t)\frac{1}{4f_\pi^4}s\Pi_V(s)\right.\\
&\left.+2\text{ permutation}\right]\\
&\Rightarrow -N_\pi\frac{st}{2f_\pi^4}[\Pi_V(s)+\Pi_V(t)],
\end{aligned}
\tag{B4}
$$

where

$$\Pi_V(q^2) = c_1 + \frac{1}{72\pi^2} + \frac{1}{3}\left(1 - \frac{4m_\pi^2}{q^2}\right)(\mathcal{J}(q^2) - \hat{c}_1) \tag{B5}$$

and

$$\mathcal{J}(q^2) = \hat{c}_1 + \frac{1}{16\pi^2}\theta(q^2 - 4m_\pi^2)\left(2 + \sqrt{1 - \frac{4m_\pi^2}{q^2}}\left[\ln\left|\frac{\sqrt{1 - 4m_\pi^2/q^2} - 1}{\sqrt{1 - 4m_\pi^2/q^2} + 1}\right| + i\pi\right]\right). \tag{B6}$$

In this work, we take the mean value of the counter term $c_1 = 0.035$ and $\hat{c}_1 = 0.023$ [34]. The scalar contribution can be rewritten as

$$\mathcal{T}_{\text{scalar}} = \sum_{a=d,b=c}\left[\frac{2m_\pi^2}{f_\pi^4}\delta^{ac}\delta^{bd}\left(s\mathcal{J}(s) - \frac{5}{4}m_\pi^2\mathcal{J}(s)\right) + 2 \text{ permutation}\right]$$

$$\Rightarrow \frac{2N_\pi m_\pi^2}{f_\pi^4}\left(s\mathcal{J}(s) + t\mathcal{J}(t) - \frac{5}{4}m_\pi^2[\mathcal{J}(s) + \mathcal{J}(t) + N_\pi\mathcal{J}(0)]\right). \tag{B7}$$

The remaining contribution can be rewritten as

$$\mathcal{T}_{\text{rest}} = \sum_{a=d,b=c}\left[-\frac{i}{f_\pi^4}k_1^\alpha k_2^\beta p_1^\gamma p_2^\delta \int d^4y_1 d^4y_2 d^4y_3\, e^{-ik_1\cdot y_1 + ik_2\cdot y_2 - ip_1\cdot y_3}\right]\langle 0|\,T^*\left[\mathbf{j}_{A\alpha}^a(y_1)\,\mathbf{j}_{A\beta}^b(y_2)\,\mathbf{j}_{A\gamma}^c(y_3)\,\mathbf{j}_{A\delta}^d(0)\right]|0\rangle_{\text{conn}}\right]$$

$$\Rightarrow \frac{N_\pi(2 + N_\pi)}{4f_\pi^4}\left[(s - 2m_\pi^2)^2\mathcal{J}(s) + (t - 2m_\pi^2)^2\mathcal{J}(t) + 4m_\pi^4\mathcal{J}(0)\right]. \tag{B8}$$

APPENDIX C: PARTONIC QUARK SUSCEPTIBILITY

The partonic flavor susceptibility is summarized following the same arguments as those developed for the hadronic parts in Eq. (35). One can start with flavor charge fluctuations

$$\langle\mathbf{Q}_f^2\rangle = \langle\mathbf{Q}_f^2\rangle_q + \langle\mathbf{Q}_f^2\rangle_{qq} + \cdots \tag{C1}$$

with

$$\langle\mathbf{Q}_f^2\rangle_q = \int dq(k)\,\langle q^{ai}(k)|\mathbf{Q}_f^2|q^{ai}(k)\rangle = 4N_c V_3\int\frac{d^3k}{(2\pi)^3}n_F(E) \tag{C2}$$

and

$$\langle\mathbf{Q}_f^2\rangle_{qq} = -\frac{1}{2!}\int dq(k_1)dq(k_2)\left(\langle q^{ai}(k_1)|\mathbf{Q}_f^2|q^{bj}(k_2)\rangle\langle q^{bj}(k_2)|q^{ai}(k_1)\rangle + a,i,k_1 \leftrightarrow b,j,k_2\right)$$

$$+ \frac{1}{2!}\int dq(k_1)dq(k_2)\,\text{Im}\langle q^{ai}(k_1)q^{bj}(k_2)|\,(\mathbf{S} - \mathbf{1})\,\mathbf{Q}_f^2|q^{ai}(k_1)q^{bj}(k_2)\rangle. \tag{C3}$$

The index a is for flavor and the index i is short for color, spin, particle, and antiparticle. The integrals count the number of massless (scalar) fermions in phase space

$$\int dq(k) = \int\frac{d^3k}{(2\pi)^3}\frac{n_F(E)}{2E}. \tag{C4}$$

In the the disconnected matrix element the minus sign is from the antisymmetric switch of the quarks. The connected contribution is the forward quark-quark scattering amplitude $\mathcal{T}_{qq}$. Thus

$$\langle\mathbf{Q}_f^2\rangle_{qq} = -4N_c V_3\int\frac{d^3k}{(2\pi)^3}n_F^2(E) + \frac{2}{2!}\int dq(k_1)dq(k_2)\,(2\pi)^4\,\delta(k_1 + k_2 - (k_1 + k_2))\,\text{Re}\mathcal{T}_{qq}^{ai,bj}(k_1,k_2) \tag{C5}$$

so that

$$\chi_f \approx \frac{4N_c}{T}\int\frac{d^3k}{(2\pi)^3}n_F(1 - n_F) + \frac{1}{T^2}\int dq(k_1)dq(k_2)\text{Re}\mathcal{T}_{qq}^{ai,bj}(k_1,k_2). \tag{C6}$$

For massless quarks, the first term gives the leading QGP contribution $\chi_f = (N_c/3)T^2$.

[1] A. Adare *et al.* (PHENIX Collaboration), Phys. Rev. Lett. **109**, 122302 (2012).
[2] F. Geurts for the STAR Collaboration, Proceedings of the 29th Winter Workshop on Nuclear Dynamics (WWND 2013), Squaw Valley, CA, arXiv:1305.5447.
[3] D. Lohner for the ALICE Collaboration, arXiv:1212.3995.
[4] H. van Hees, C. Gale, and R. Rapp, Phys. Rev. C **84**, 054906 (2011).
[5] R. Rapp, J. Phys.: Conf. Ser. **420**, 012017 (2013).
[6] R. Rapp, Adv. High Energy Phys. **2013**, 148253 (2013).
[7] R. Rapp, Proceedings of 8th International Workshop on Critical Point and Onset of Deconfinement (CPOD13), March 11–15, 2013, Napa, California, USA, arXiv:1306.6394.
[8] C. Shen, U. W. Heinz, J.-F. Paquet, I. Kozlov, and C. Gale, arXiv:1308.2111.
[9] C. Shen, U. Heinz, J.-F. Paquet, and C. Gale, Phys. Rev. C **89**, 044910 (2014).
[10] G. Vujanovic, C. Young, B. Schenke, R. Rapp, S. Jeon, and C. Gale, Phys. Rev. C **89**, 034904 (2014).
[11] J. V. Steele, H. Yamagishi, and I. Zahed, Phys. Lett. B **384**, 255 (1996).
[12] J. V. Steele, H. Yamagishi, and I. Zahed, Phys. Rev. D **56**, 5605 (1997).
[13] C.-H. Lee, H. Yamagishi, and I. Zahed, Phys. Rev. C **58**, 2899 (1998).
[14] K. Dusling, D. Teaney, and I. Zahed, Phys. Rev. C **75**, 024908 (2007).
[15] K. Dusling and I. Zahed, Phys. Rev. C **80**, 014902 (2009).
[16] K. Dusling and I. Zahed, Phys. Rev. C **82**, 054909 (2010).
[17] L. D. McLerran and T. Toimela, Phys. Rev. D **31**, 545 (1985).
[18] T. H. Hansson and I. Zahed, QCD sum rules at high temperature, PRINT-90-0339 (STONY-BROOK) (1990).
[19] C.-H. Lee, J. Wirstam, I. Zahed, and T. H. Hansson, Phys. Lett. B **448**, 168 (1999).
[20] G. Başar, D. E. Kharzeev, and E. V. Shuryak, Phys. Rev. C **90**, 014905 (2014).
[21] H.-T. Ding, A. Francis, O. Kaczmarek, F. Karsch, E. Laermann, and W. Soeldner, Phys. Rev. D **83**, 034504 (2011).
[22] B. B. Brandt, A. Francis, H. B. Meyer, and H. Wittig, J. High Energy Phys. 03 (2013) 100.
[23] H.-T. Ding *et al.*, Proceedings of Xth Quark Confinement and the Hadron Spectrum, October 8–12, 2012, TUM Campus Garching, Munich, Germany, arXiv:1301.7436.
[24] M. Dey, V. L. Eletsky, and B. L. Ioffe, Phys. Lett. B **252**, 620 (1990).
[25] Z. Huang, Phys. Lett. B **361**, 131 (1995).
[26] K. Dusling, Ph.D. thesis, Stony Brook University, 2008, arXiv:0901.2027.

[27] H. A. Weldon, Phys. Rev. D **42**, 2384 (1990).
[28] A. Adare *et al.* (PHENIX Collaboration), Phys. Rev. C **81**, 034911 (2010).
[29] A. Adare *et al.* (PHENIX Collaboration), Phys. Rev. Lett. **104**, 132301 (2010).
[30] A. A. Abrikosov, L. P. Gorkov, and I. E. Dzyaloshinski, in *Methods of Quantum Field Theory in Statistical Physics*, translated and edited by R. A. Silverman (Dover Publishing, Inc., New York, 1975).
[31] O. Kaczmarek and M. Müller, Proceedings of the 31st International Symposium on Lattice Field Theory (Lattice 2013), 29 July–3 August 2013, Mainz, Germany, arXiv:1312.5609.
[32] Y. Burnier and M. Laine, Eur. Phys. J. C **72**, 1902 (2012).
[33] J. M. Torres-Rincon, F. J. Llanes-Estrada, and A. Dobado, Ph.D. thesis, Madrid University, 2012, arXiv:1205.0782.
[34] H. Yamagishi and I. Zahed, Ann. Phys. (NY) **247**, 292 (1996).
[35] H. Yamagishi and I. Zahed, Phys. Rev. D **53**, R2288 (1996).
[36] P. Arnold, G. D. Moore, and L. G. Yaffe, J. High Energy Phys. 012 (2001) 009.
[37] C. Adami, T. Hatsuda, and I. Zahed, Phys. Rev. D **43**, 921 (1991).
[38] S. Narison, Phys. Lett. B **673**, 30 (2009).
[39] E. Braaten, R. D. Pisarski, and T. C. Yuan, Phys. Rev. Lett. **64**, 2242 (1990).
[40] H. A. Weldon, Phys. Rev. D **40**, 2410 (1989).
[41] Y. Yin, arXiv:1312.4434.
[42] G. Aarts, C. Allton, J. Foley, S. Hands, and S. Kim, Phys. Rev. Lett. **99**, 022002 (2007).
[43] A. Amato, G. Aarts, C. Allton, P. Giudice, S. Hands, and J.-I. Skullerud, Phys. Rev. Lett. **111**, 172001 (2013).
[44] T. Steinert and W. Cassing, Phys. Rev. C **89**, 035203 (2014).
[45] W. Cassing, O. Linnyk, T. Steinert, and V. Ozvenchuk, Phys. Rev. Lett. **110**, 182301 (2013).
[46] R. Marty, E. Bratkovskaya, W. Cassing, J. Aichelin, and H. Berrehrah, Phys. Rev. C **88**, 045204 (2013).
[47] P. Arnold, G. D. Moore, and L. G. Yaffe, J. High Energy Phys. 11 (2000) 001.
[48] P. Arnold, G. D. Moore, and L. G. Yaffe, J. High Energy Phys. 05 (2003) 051.
[49] V. L. Eletsky, P. J. Ellis, and J. I. Kapusta, Phys. Rev. D **47**, 4084 (1993).
[50] A. Bazavov, H.-T. Ding, P. Hegde, F. Karsch, C. Miao, S. Mukherjee, P. Petreczky, C. Schmidt, and A. Velytsky, Phys. Rev. D **88**, 094021 (2013).
[51] M. Natsuume and T. Okamura, Phys. Rev. D **77**, 066014 (2008); **78**, 089902(E) (2008).
[52] Y. Akamatsu, H. Hamagaki, T. Hatsuda, and T. Hirano, Phys. Rev. C **85**, 054903 (2012).
[53] G. D. Moore and D. Teaney, Phys. Rev. C **71**, 064904 (2005).
[54] S. Cao, G.-Y. Qin, and S. A. Bass, Phys. Rev. C **88**, 044907 (2013).